nature structural & molecular biology

Subunit connectivity, assembly determinants and architecture of the yeast exocyst complex

Margaret R Heider[1], Mingyu Gu[2], Caroline M Duffy[1], Anne M Mirza[1], Laura L Marcotte[1,6], Alexandra C Walls[1], Nicholas Farrall[2], Zhanna Hakhverdyan[3], Mark C Field[4], Michael P Rout[3], Adam Frost[2,5] & Mary Munson[1]

The exocyst is a hetero-octameric complex that has been proposed to serve as the tethering complex for exocytosis, although it remains poorly understood at the molecular level. Here, we purified endogenous exocyst complexes from *Saccharomyces cerevisiae* and showed that they are stable and consist of all eight subunits with equal stoichiometry. Using a combination of biochemical and auxin induced–degradation experiments in yeast, we mapped the subunit connectivity, identified two stable four-subunit modules within the octamer and demonstrated that several known exocyst-binding partners are not necessary for exocyst assembly and stability. Furthermore, we visualized the structure of the yeast complex by using negative-stain electron microscopy; our results indicate that the exocyst exists predominantly as a stable, octameric complex with an elongated architecture that suggests that the subunits are contiguous helical bundles packed together into a bundle of long rods.

© 2015 Nature America, Inc. All rights reserved.

Exocytosis is the evolutionarily conserved pathway by which protein and lipid cargos are trafficked from intracellular compartments to the plasma membrane in membrane-bound vesicles. This pathway is essential for cellular growth and division as well as for specialized processes such as cell migration, ciliogenesis and autophagy[1]. To maintain the fidelity of the secretory pathway, numerous conserved protein families regulate every step of the process[2]. Tethering factors, including the multisubunit tethering complexes (MTCs), serve as the first long-range, reversible connection between a vesicle and its target membrane[3,4]. However, in many cases, experimental evidence demonstrating tethering by these factors is lacking[5]. Tethers have been proposed to provide specificity for vesicle targeting, but they may also assume a more active role in regulating SNARE-mediated membrane fusion[3,6–8].

The exocyst complex is the MTC for secretory vesicles at the plasma membrane, and it contains eight subunits—Sec3, Sec5, Sec6, Sec8, Sec10, Sec15, Exo70 and Exo84—all of which have orthologs in eukaryotes including yeasts and humans[9–14]. Yeast exocyst mutants display severe growth and secretion defects and accumulate post-Golgi secretory vesicles in the cytoplasm[15,16]. Similarly, null mutants in mice and flies exhibit embryonic and larval lethality, respectively[17,18]. Although previous studies have revealed requirements for the exocyst in many critical cellular processes involving polarized vesicle trafficking, the structure and mechanisms of tethering by the exocyst remain unresolved[1].

Similarly to other tethering factors, the exocyst is a peripheral membrane protein complex that interacts with numerous GTPases, SNAREs, phospholipids and the vesicle-transport motor myosin V[1,3,19,20]. The exocyst has been proposed to interact with vesicles through Sec15 binding to the Rab GTPase Sec4 and myosin V, as well as Sec6 binding to the v-SNARE Snc[16,19,21]. On the target-membrane side, both Sec3 and Exo70 interact with Rho GTPases and phosphatidylinositol 4,5-bisphosphate[22–26], and Sec6 may interact with an as-yet-unidentified 'anchor' factor at the plasma membrane[27]. It is through this myriad of connections that the exocyst has been predicted to selectively capture secretory vesicles and tether them to the plasma membrane. A current model for exocyst function proposes that a subcomplex of exocyst subunits in *S. cerevisiae* is carried on vesicles to another subcomplex at the plasma membrane, and assembly of these subcomplexes drives vesicle tethering[28]. However, this model has not yet been validated biochemically, nor have the putative subcomplexes been identified. Whether regulated assembly of the exocyst is required for tethering and SNARE-complex regulation in yeast or other organisms, and whether these mechanisms differ between different species, are important unanswered questions.

Mechanistic models for exocyst function must be informed by the structural arrangement of exocyst subunits. Crystal structures of several exocyst subunits reveal a strikingly similar motif of contiguous helical bundles that pack together into long rods, thus classifying the exocyst within the evolutionarily conserved complexes associated with tethering containing helical rods (CATCHR) family[3,20]. Numerous pairwise subunit interactions have been identified via yeast two-hybrid assays, immunoprecipitations and *in vitro* binding experiments using recombinant and *in vitro*–translated proteins[20,29]. To examine the architecture and regulation of exocyst assembly, we developed a new robust exocyst purification method to reproducibly

[1]Department of Biochemistry and Molecular Pharmacology, University of Massachusetts Medical School, Worcester, Massachusetts, USA. [2]Department of Biochemistry, University of Utah, Salt Lake City, Utah, USA. [3]Laboratory of Cellular and Structural Biology, The Rockefeller University, New York, New York, USA. [4]Division of Biological Chemistry and Drug Discovery, University of Dundee, Dundee, UK. [5]Department of Biochemistry and Biophysics, University of California, San Francisco, San Francisco, California, USA. [6]Present address: Department of Natural Sciences, Assumption College, Worcester, Massachusetts, USA. Correspondence should be addressed to M.M. (mary.munson@umassmed.edu).

Received 15 May; accepted 19 November; published online 14 December 2015; doi:10.1038/nsmb.3146

isolate stable exocyst complexes from *S. cerevisiae*. Using an auxin-inducible degradation (AID) system to deplete single subunits, we mapped the connectivity of the eight subunits and determined that most of the subunits are required for the association of two assembly modules within the exocyst. In contrast, depletion of known binding partners had no effect on the assembly status of the exocyst. Here we present the first structure, to our knowledge, of a fully assembled CATCHR MTC—we determined the structure of the fully assembled exocyst through negative-stain EM and two-dimensional (2D) averaging. Furthermore, we demonstrate that exocyst complexes are stoichiometric with no detectable subcomplexes; therefore, we propose that the yeast exocyst functions predominantly as a fully assembled complex.

RESULTS

Purification of intact yeast exocyst complexes

Biochemical and structural studies of the intact exocyst complex have previously been limited by preparations with poor yield, stability and purity (refs. 9,10,30–32 and M.M., unpublished data). In order to answer critical questions regarding the architecture of the yeast exocyst complex and its putative assembly dynamics, we have developed an improved protocol for isolating the entire native complex from yeast extract[33,34]. To maintain endogenous expression levels and function, we fused C-terminal Protein A (PrA) affinity tags to each exocyst subunit individually by integrating DNA encoding PrA at each genomic locus, creating eight different tagged haploid *S. cerevisiae* strains (**Supplementary Table 1**). The C-terminal PrA tags did not confer growth defects (**Supplementary Fig. 1a**), thus demonstrating that each of the tagged subunits was functional. We grew yeast strains, harvested them in log phase as frozen noodles and lysed them with a planetary ball mill grinder (Online Methods). We then resuspended the lysate powder in a physiological buffer, incubated the lysate with rabbit IgG–conjugated magnetic beads and eluted bound proteins from the beads either by proteolytic digestion or by denaturation with SDS loading buffer (**Fig. 1**). We confirmed exocyst subunit identities on the basis of the molecular-weight shift of the PrA tag in SDS-PAGE (**Fig. 1**), MALDI-MS and western blot analyses (data not shown).

We isolated intact exocyst complexes from yeast extracts by using each of the eight subunits as the PrA-tagged purification handle. The eight exocyst subunits copurified with equal stoichiometry, as detected by both Coomassie-stained SDS-PAGE and densitometry with Krypton fluorescent protein stain (**Fig. 1**), consistently with results from earlier reports[9,31]. We next asked whether the complexes purified by this method undergo disassembly and reassembly during the purification. When we mixed Sec10-GFP lysate with either Sec3-PrA or Exo70-PrA lysates and subsequently purified the exocyst complexes, we detected no Sec10-GFP in either pulldown, thus indicating that no exchange or assembly of subunits occurred during the incubation (1 h at 4 °C) (**Supplementary Fig. 1b**); these results are consistent with those from our previous studies[27]. Therefore, the purified complexes represent the state of the endogenous complex at the time of cell lysis.

The improved yield and purity of our exocyst preparations are the result of decreased proteolysis from cryogenic lysis (**Supplementary Fig. 1c**) and the use of rabbit IgG–conjugated magnetic beads, which have a high affinity for PrA[35,36]. Additionally, protease cleavage allowed for increased purity and native elution of untagged complexes for structural studies (**Supplementary Fig. 1d**). We detected substoichiometric levels of copurifying proteins by MS and krypton fluorescent protein staining, but they appeared to primarily be highly expressed, nonspecific contaminants or previously detected binding partners, including Rtn1 (ref. 31).

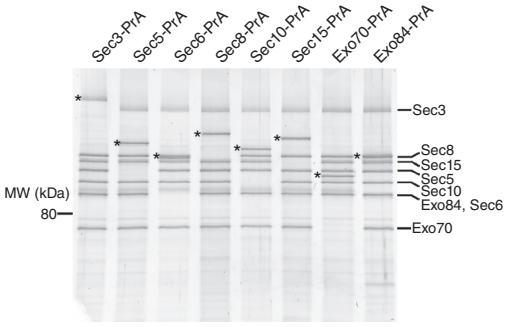

Figure 1 Purification of intact yeast exocyst complexes. Purified complexes were separated by SDS-PAGE and visualized by Krypton staining. The asterisks correspond to the PrA-tagged exocyst subunit used as a purification handle (which shifts the protein molecular weight (MW) by 25 kDa). Owing to phosphorylation, both the Sec3 and Exo84 protein bands often migrate as multiple species, which appear as slightly smeared bands on SDS-PAGE. The resuspension buffer used was 50 mM HEPES, pH 7.4, and 300 mM NaCl, plus protease inhibitors. Full-size images for this and subsequent cropped gel images are shown in **Supplementary Data Set 1**.

We next tested the functionality of our exocyst preparations by western blotting for known exocyst-interacting partners (**Supplementary Fig. 2**). The improved yield and rapid, gentle purification procedure allowed detection of binding of Sec1, Myo2 and Snc1/2 (redundant paralogs) to the exocyst. Previous studies have revealed an interaction of the exocyst subunit Sec6 with both Sec1 and Snc2 (refs. 7,21), and Sec15 with Myo2 (ref. 19). Here, we show that these proteins can be pulled down with tagged exocyst subunits that are not their direct binding partners, thus suggesting that these interactions occur within the context of the assembled complex.

Using Sec15-PrA as the purification handle, we monitored exocyst integrity under a variety of pH and salt conditions (**Fig. 2a**). The presence of reducing agents had no effect on complex recovery, and the complex was stable across a range of pH solutions, in contrast to results from previous studies[30]. Increasing the pH above 8.5 rendered purified exocyst complexes sensitive to salt concentrations ≥300 mM. In Tris, pH 8.5, and ≥500 mM salt, only Sec15 and Sec10 remained bound together, thus indicating a strong physical interaction between these two subunits that is consistent with results of earlier studies[16].

The exocyst complex peripherally associates with vesicles and the plasma membrane[37]. We therefore tested the effect of detergents, particularly whether the stoichiometry changes because of the solubilization of membrane-bound subcomplexes or the disruption of intersubunit interactions. We tested several nonionic detergents including NP-40 (IGEPAL), Tween-20 and Triton X-100, and none of the detergents affected the overall yield of assembled exocysts or the relative stoichiometry of the subunits (**Fig. 2b**). In contrast, the exocyst was severely disrupted by sodium cholate, a strong anionic detergent. Together, these results indicate that varying the ionic strength of the resuspension buffer has a pronounced effect on exocyst integrity, suggesting that ionic interactions may be a major stabilizing force for intersubunit connections.

We used our pulldown assay to identify stable intracomplex interactions within the endogenous exocyst complex, using partially destabilizing buffer conditions, with each of the eight PrA-tagged exocyst subunits (**Fig. 2c**). Several stable subunit pairs emerged: Sec3–Sec5, Sec6–Sec8 and Sec10–Sec15. Neither Exo70 nor Exo84 bound tightly to any of the other subunits under these

© 2015 Nature America, Inc. All rights reserved.

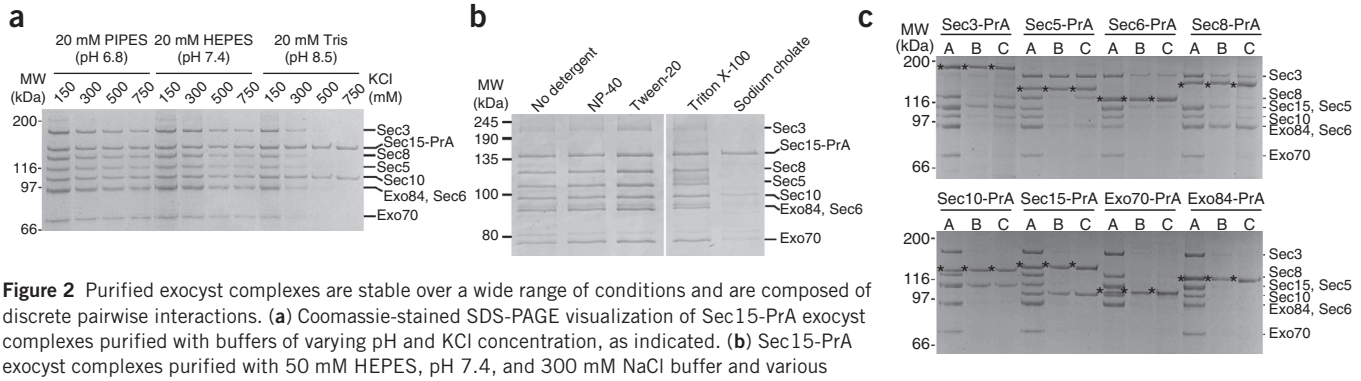

Figure 2 Purified exocyst complexes are stable over a wide range of conditions and are composed of discrete pairwise interactions. (**a**) Coomassie-stained SDS-PAGE visualization of Sec15-PrA exocyst complexes purified with buffers of varying pH and KCl concentration, as indicated. (**b**) Sec15-PrA exocyst complexes purified with 50 mM HEPES, pH 7.4, and 300 mM NaCl buffer and various commonly used detergents at the following concentrations: 0.1% NP-40, 0.1% Tween-20, 1% Triton X-100 and 20 mM sodium cholate. (**c**) Destabilizing buffer conditions were used with each exocyst subunit as a PrA purification handle to isolate subcomplexes and stable subunit pairs. A, 20 mM PIPES, pH 6.8, and 300 mM KCl; B, 20 mM Tris, pH 8.5, and 500 mM KCl; C, 20 mM Tris, pH 8.5, 300 mM KCl, and 500 mM urea. Asterisks correspond to the PrA-tagged subunit.

destabilizing conditions. Although several of these pairwise interactions had previously been identified[16,29,38,39], the relative stabilities of the subunit pairs compared to other intersubunit interactions were unknown.

Subunit connections and intracomplex assembly determinants

We applied a more targeted approach to answer additional architectural questions: How are these pairs of subunits assembled into the overall connectivity map of the assembled exocyst? Which of these intersubunit interactions are functionally important for maintaining exocyst integrity? Are some subunits more important for interactions with binding partners on the plasma membrane and vesicle? We decided to selectively eliminate individual exocyst subunits to define their role in maintaining overall complex assembly. All exocyst subunits except Sec3 are encoded by essential genes and therefore cannot be deleted from the yeast genome[39,40]. We tested the temperature-sensitive (ts) mutants *sec3-2*, *sec5-24*, *sec6-4*, *sec8-6* and *sec10-2* and used Sec15-PrA as the purification handle. Only *sec8-6* had a major effect on exocyst integrity at the restrictive temperature (data not shown). These results were difficult to interpret, however, because the ts alleles vary in their severity and in the amount of destabilization or degradation of the mutant protein. Previous studies using a similar panel of exocyst ts mutants have shown greater disassembly for several of the mutants than we observed, even at the permissive temperature[10]. These differences are probably due to proteolysis of exocyst subunits during spheroplasting lysis, which destabilizes the complex (**Supplementary Fig. 1c**). To overcome these challenges, we used an AID system to specifically remove each individual exocyst subunit.

This degron system uses the IAA17 AID sequence from *Arabidopsis thaliana*, which is fused to each exocyst subunit. When this tagged protein is coexpressed with the auxin receptor OsTIR1, exposure to the plant hormone auxin leads to rapid proteosomal degradation of the tagged subunit[41,42] (**Fig. 3a**). Addition of these tags to the C-terminal ends of exocyst subunits conferred no growth defects on their own, but when cells were grown on plates containing auxin (indole-3-acetic acid, IAA), all exocyst-AID strains were inviable except for Sec3-AID (**Fig. 3b**). We confirmed rapid and specific IAA-induced degradation of individual exocyst subunits in liquid culture by western blot analyses of yeast lysates. Each exocyst subunit was degraded to <12% of the starting level within 60 min of IAA treatment (**Fig. 3c**), whereas the protein levels of the remaining subunits were mostly unchanged (**Supplementary Fig. 3**).

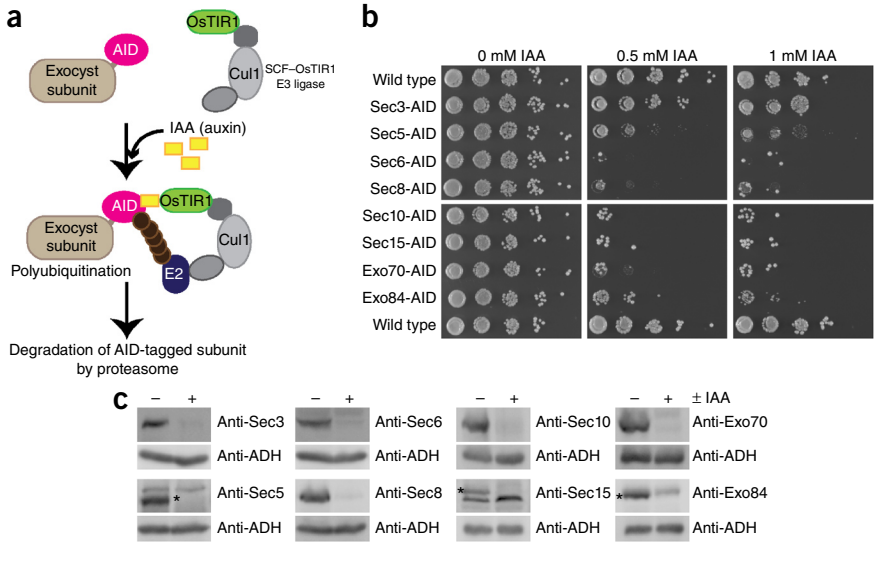

Figure 3 Use of the auxin-inducible degron (AID) system to selectively degrade essential exocyst proteins from yeast. (**a**) Schematic of the AID system. The AID tag from *A. thaliana* was fused to the C terminus of exocyst subunits at their genomic locus in yeast strains constitutively expressing OsTIR1 (F-box transport inhibitor response 1) protein. Upon treatment with the natural plant hormone auxin (indole-3-acetic acid (IAA)), the SCF–OsTIR1 E3 ubiquitin ligase complex is activated and subsequently recruits E2 ubiquitin conjugating enzymes for polyubiquitination of the AID-tagged protein. The AID-tagged protein is then rapidly degraded by the proteasome[41,42]. (**b**) Serial-dilution growth assay of AID-tagged exocyst strains on yeast peptone dextrose (YPD) plates containing the indicated amount of IAA. Suppressor colonies can be seen in some dilutions. (**c**) Western blotting of lysates, confirming degradation of exocyst subunits in these strains. Minus denotes untreated strains, and plus denotes strains treated with IAA. All subunits were degraded to <10–12% of the starting protein level. Asterisks indicate the AID-tagged exocyst subunit in blots in which antibodies also bind nonexocyst proteins.

© 2015 Nature America, Inc. All rights reserved.

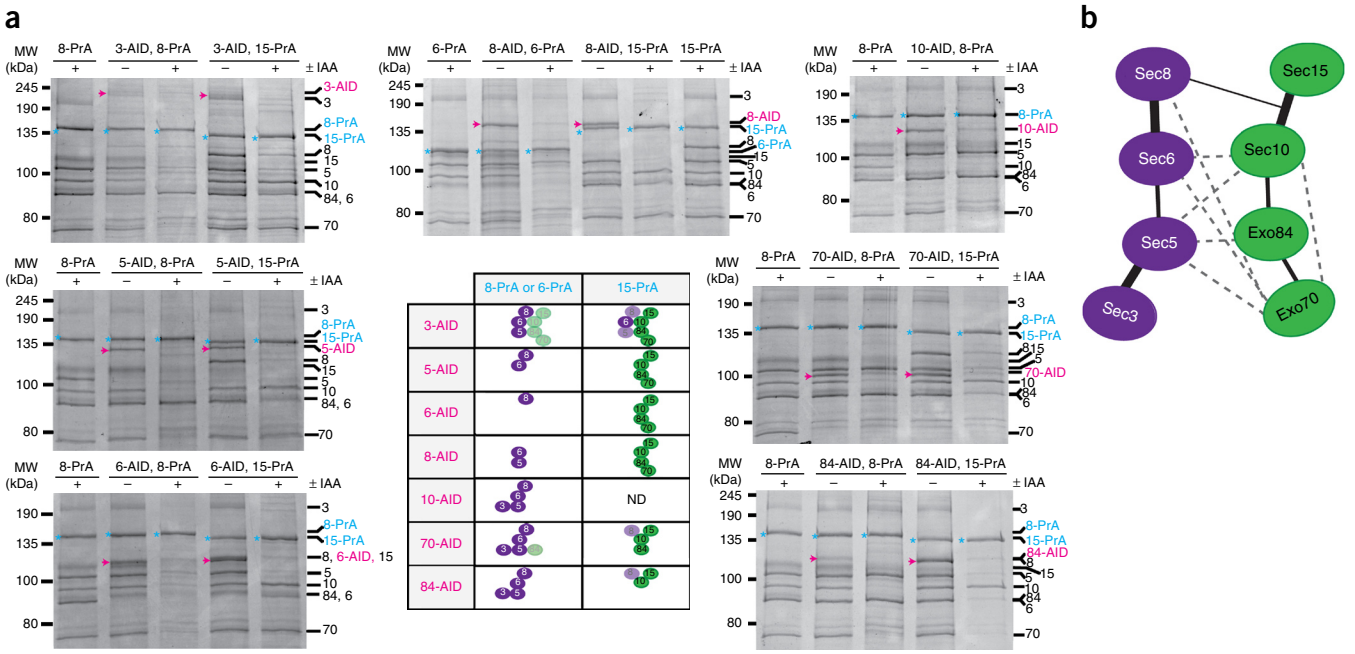

Figure 4 Most exocyst subunits are critical for maintaining the assembly of two four-subunit modules within the full octameric complex. (**a**) SDS-PAGE and Coomassie staining of exocyst complexes purified with the indicated PrA purification handles (blue) from yeast strains in which one AID-tagged subunit (magenta) was degraded. Minus denotes untreated strains, and plus denotes strains treated with IAA. For simplicity, exocyst subunits are denoted by their associated number. Degradation of six of the subunits tested led to the complete separation of exocyst complexes into two four-subunit modules: 3–5–6–8 and 10–15–70–84, with the connections depicted in the central table. The combination of Sec10-AID and Sec15-PrA was not determined (ND). Faded ovals represent subunits that showed partial loss from the complex. (**b**) Model depicting the subunit connectivity within and between each exocyst module (green and purple). Thick lines indicate the strong pairwise connections required for stability of the assembled exocyst. The thin line depicts a putative connection between Sec8 and Sec10–Sec15 identified in the AID studies, although Sec8's direct binding partner within this pair is not known. Dashed lines represent weaker interactions identified in previous *in vitro* studies (summarized in ref. 20).

To assess the role of each individual subunit in maintaining the assembly of the endogenous exocyst complex, we combined this AID system with our PrA-tag purification approach. We added genomic C-terminal PrA tags to Sec8, Sec15 or Sec6 in strains already expressing an AID-tagged exocyst subunit and OsTIR1. We tested two different PrA-tag handles for each AID-tagged subunit to determine the fate of each of the exocyst subunits. Most of the dual-tagged exocyst strains grew normally but were inviable on IAA plates, as expected (**Supplementary Fig. 4a**). Unexpectedly, the strain with Sec10-AID and Sec15-PrA showed no growth defect on IAA plates and no loss of Sec10-AID in IAA-containing liquid culture; similarly, Sec15-AID was not degraded in combination with PrA-tagged exocyst subunits (data not shown). We speculate that the lack of degradation in these strains may be due to masking of the AID tag by the 25-kDa PrA tag on a neighboring exocyst subunit.

We purified the exocyst complex from both untreated and IAA-treated cultures for each exocyst-AID-PrA combination strain and visualized the complexes by Coomassie staining and western blotting (**Fig. 4a** and **Supplementary Fig. 4b**). Surprisingly, the loss of Sec5, Sec6, Sec8, Sec10, Exo70 or Exo84 resulted in the exocyst complex splitting into two distinct, stable modules: Sec3–Sec5–Sec6–Sec8 (3–5–6–8) and Sec10–Sec15–Exo70–Exo84 (10–15–70–84). The results from the different combinations of AID and PrA tags indicate the division of the exocyst structure into two modules (summarized in **Fig. 4a**). Loss of Sec3 had the least destabilizing effect on exocyst-complex assembly. Degradation of each of the other subunits had distinct effects on its own module, depending on the strength and connectivity of its interactions with its partners, but had no effect on the integrity of the opposing module.

We found that the individual assembly of each module is predominantly based on the association of three stable subunit pairs (3–5, 6–8 and 10–15), instead of requiring the cooperative assembly of all four subunits together. If exocyst assembly were cooperative, we would expect to observe complete disassembly of all four subunits from each module upon loss of one subunit; instead, we generally found subcomplexes containing two or three subunits (for example, Sec6 and Sec5 remain bound after Sec8 is degraded). This finding is consistent with our earlier biochemistry results demonstrating that these subunit pairs are stable enough to be copurified (**Fig. 2c**). Therefore, the most robust interactions within the complex exist between pairs of subunits, and the overall assembly appears to be mediated by a network of weaker interactions. Several additional rules for exocyst assembly can be drawn from these results (**Fig. 4b**). Sec8 requires Sec6 for assembly into the complex. Sec5 is required for Sec3's assembly and for the stable interaction of Sec3 with Sec6 and Sec8. In the absence of Sec8, there was also loss of Sec3 from Sec5–Sec6, thus suggesting either a potential interaction between Sec3 and Sec8 or a potential conformational change that weakens Sec3's association with Sec5–Sec6. In the case of the other module, Sec10 and Sec15 are a stable pair that require Exo84 for their association with Exo70. Although we were unable to test this hypothesis, we predict that degradation of Sec15 would not disrupt Sec10's connection with Exo84 and Exo70, because Sec15's only known stable exocyst partner is Sec10 (ref. 16) (**Fig. 2**).

These studies provide only a few clues as to the interconnections between the modules. All subunits are required for the assembly of the two modules, including Exo70 and Exo84, which is perhaps surprising

© 2015 Nature America, Inc. All rights reserved.

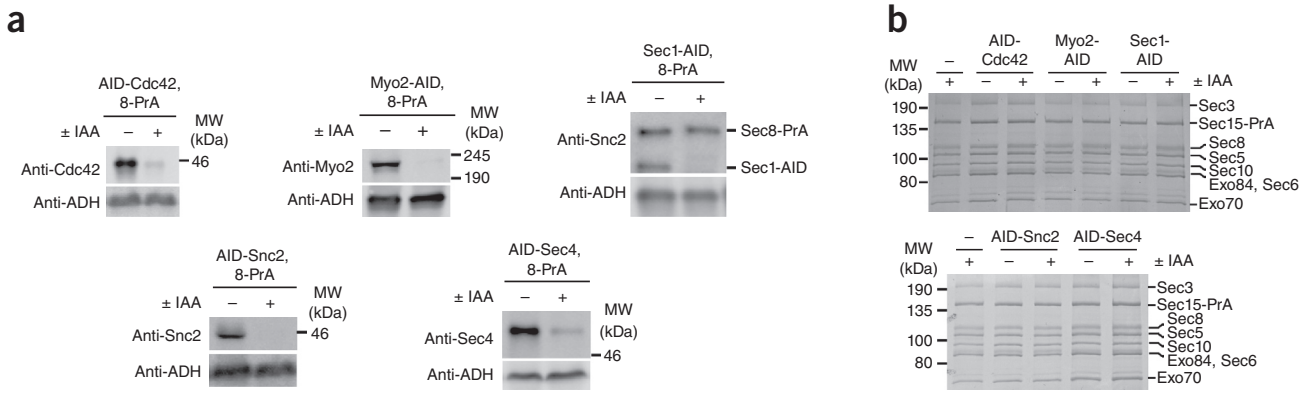

Figure 5 Depletion of known exocyst-binding partners does not affect the assembly of the exocyst complex. (**a**) Western blotting of exocyst-binding partners Cdc42, Myo2, Sec1, Snc2 (in the *snc1*Δ strain background) and Sec4, which were AID-tagged in strains expressing Sec8-PrA and constitutively expressing OsTIR1. Minus denotes untreated strains, and plus denotes strains treated with IAA for 60 min. Western blots with antibodies specific to the AID-tagged protein of interest demonstrate degradation of these proteins from yeast lysate. In the Sec1 blot, the Sec1 antibody also reacts with the PrA tag on Sec8-PrA. (**b**) Exocyst complexes purified with Sec8-PrA as the purification handle from untreated (–) and IAA-treated (+) yeast lysates.

in light of our biochemical studies, which demonstrated that Exo70 and Exo84 are not tightly associated with any other subunits of the complex (**Fig. 2**). We propose that the interconnections between the modules are made up of a network of weaker subunit-subunit interactions, although we cannot rule out that the degradation of a subunit from one module may alter the structure of its respective subcomplex, thus making it incompatible for binding the opposing module. Other previously identified subunit interactions may contribute to this intermodule network[20,29], but their relative contributions remain to be tested (**Fig. 4b**).

Exocyst-binding partners have no effect on exocyst assembly

We wondered whether any additional binding partners would be necessary to maintain this stable assembly. However, we detected only substoichiometric amounts of known binding partners in our exocyst preparations, thus suggesting that these partners do not need to remain bound to maintain exocyst integrity (**Fig. 1** and **Supplementary Fig. 2**).

A major unresolved question is how the exocyst assembles *in vivo* and whether additional factors are required for regulating this assembly. Selective elimination of individual exocyst-interacting partners along the late secretory pathway might identify subcomplexes, thereby indicating a failure of the complex to fully assemble. To test this idea, we again used our AID-tag approach to deplete the master polarity regulator Cdc42 (ref. 43), the type V myosin motor Myo2 (ref. 19), the SNARE regulator Sec1 (ref. 44), the v-SNARE Snc2 (ref. 21) and the Rab GTPase Sec4 (ref. 16) (**Supplementary Fig. 5a**). The functional consequences of each of these interactions are not known, and it is unclear at which stage of exocytosis these interactions occur[7,23,39,45].

We treated the AID-tagged partner strains with IAA for 1 h, a time sufficient for numerous rounds of vesicle delivery and fusion in *S. cerevisiae*[46]. Degradation of Sec1 induced a severe vesicle accumulation phenotype, as expected[47], whereas degradation of Myo2 and Cdc42 caused a milder secretion defect consistent with results from previous reports[43,48] (**Supplementary Fig. 5b,c**). N-terminal AID-tagging of Snc and Sec4 resulted in severe vesicle accumulation even before IAA treatment, thus suggesting that these N-terminal tags partially impair protein function (**Supplementary Fig. 5b,c**). Using a PrA tag on Sec8, we pulled down exocyst complexes after degradation of these partners (**Fig. 5**). For each of the proteins tested, we observed that the exocyst complexes were fully assembled and stoichiometric, and they could be recovered with the same yield.

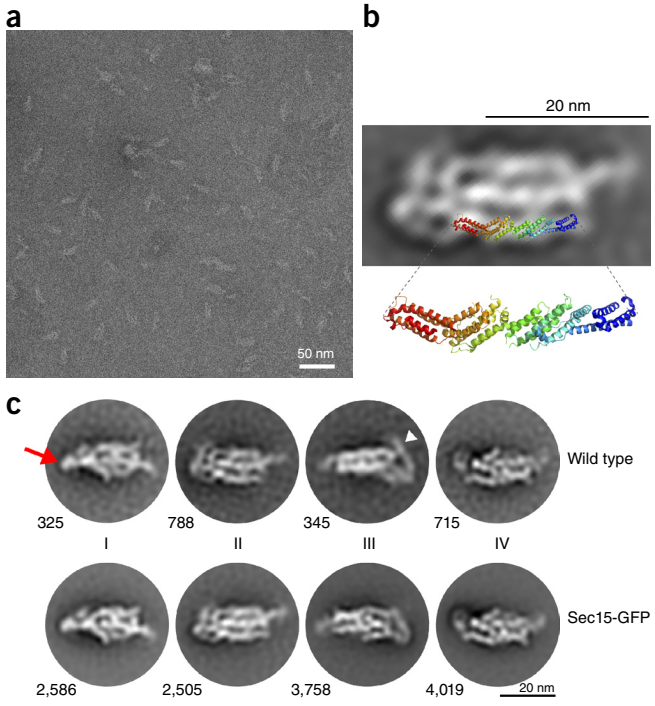

Figure 6 Negative-stain EM of purified exocyst complexes. (**a**) A representative transmission electron micrograph of Sec15-GFP exocyst complexes after negative staining in uranyl acetate. Scale bar, 50 nm. (**b**) 2D class average (Sec15-GFP), overlaid with a ribbon diagram of the structure of yeast Exo70 (residues 67–623), PDB 2B1E[51]. The orientation and position of Exo70 were arbitrarily chosen to illustrate the similarities in the length and width of the legs of the complex and Exo70. (**c**) Highly populated 2D class averages generated by unsupervised classification for both wild-type and Sec15-GFP image data sets. The number of particles per class is indicated next to each 2D average. Four apparent faces of the complex are labeled I–IV. The red arrow points to the more 'compact' end of the complex in class I, and the white arrowhead points to the more open, flexible end in class III. Scale bar, 20 nm.

© 2015 Nature America, Inc. All rights reserved.

These results indicate that none of these components are required for driving or stabilizing the assembly of exocyst complexes. Together with the preceding observations that the exocyst subunits copurify in stoichiometric complexes, these data support a model wherein the exocyst functions predominantly in a fully assembled state in actively growing cells, even under conditions in which vesicles are not being transported, and the exocyst is not interacting with its partners.

Visualization of exocyst structure by electron microscopy

Our new purification method for the yeast exocyst complex allowed us to obtain pure complexes for structural studies. We purified both Sec15-GFP and wild-type complexes and analyzed them through negative-stain EM. Raw micrographs revealed distinct particles with an ellipsoid structure approximately 25 nm in length (**Fig. 6a**). Iterative rounds of unsupervised 2D classification and class averaging revealed multiple coherent views of the exocyst complex resolved between 17-Å and 25-Å resolution (**Fig. 6b**,**c** and **Supplementary Fig. 6**). However, this averaging failed to reveal a unique density attributable to GFP, thus precluding identification of Sec15's location within the structure. At this resolution, the orientations and overall architecture of the exocyst were indistinguishable between these biologically and technically independent data sets (**Fig. 6c** and **Supplementary Fig. 6**). We observed no apparent density or class averages for smaller particles, such as subcomplexes.

The 2D class averages resolved into roughly four distinct views of the complex (**Fig. 6c** and **Supplementary Fig. 6**), which may represent four 'faces' of the complex as it interacts with the EM grid. One end of the structure (left side of each of the 2D images) appears to be more tightly packed and ordered than the other end, which appears to be more flexible, often containing a long looping 'leg' wrapping around the end (right side of each of the 2D images). Two of the faces of the complex (I and II) appear wider and contain three to four legs or columns of density packed together, whereas the two slightly narrower faces (III and IV) appear to have only two to three legs each. We speculate that the more tightly packed end of the long axis of the complex may be composed of many of the N-terminal ends of exocyst subunits, because they generally have not been amenable to biochemical studies in isolation[49]. The C-terminal ends, therefore, would be present in the more flexible, 'open' end of the structure; these regions contain many of the regions involved in binding GTPases and the plasma membrane[23,24,50,51]. The exception is Sec3, whose membrane-interaction domain is located at its N-terminal end[26,52] and may therefore lie at the flexible open end of the exocyst, in an opposite orientation to the others.

Each of the individual legs observed in the 2D class averages of the exocyst complex are ~3 nm wide. Although the N- and C-terminal ends of the subunits cannot be unambiguously identified at this resolution, we can estimate the length of the legs in the range of ~15–35 nm, with the additional long leg at the flexible end being ~25 nm longer than the others. When the crystal structure of nearly full-length yeast Exo70 (residues 67–623) is superimposed onto an arbitrarily chosen leg, the width and length of the leg are consistent with the structure, which is ~16 nm long and ~3.0–3.5 nm wide[51] (**Fig. 6b**). Exo70 is the smallest exocyst subunit (71 kDa), and the others range from 84 kDa to 155 kDa. The large size of Sec3 (155 kDa; estimated extended helical-bundle length of ~38 nm) suggests that it may be the subunit that wraps around the end of the complex (**Fig. 6c**). The other available crystal structures (Exo84CT, Sec6CT and Sec15CT) also revealed similar CATCHR family helical bundles that are ~3 nm wide; the other subunits have been predicted to have similar folds[49–51,53,54]. The subunits of the complex appear to lie in a roughly parallel arrangement to each other, as suggested by previous interaction studies[20,51,54]. Our interpretation of the 2D averages suggests that this structure represents a fully assembled complex with an estimated volume of ~1,800–2,200 nm^3. Using the volume and molecular weight of the structure of Exo70, and the assumption that all the subunits have roughly similar helical-bundle structures, we calculated a comparable volume of ~1,900 nm^3 for the octameric complex. Therefore, we suggest that our structure contains all eight subunits, consistently with the biochemical and AID experiments. Furthermore, we speculate that the wider faces containing three or four legs represent the two distinct modules identified in our AID studies, with one module as the top face and the other as the bottom face. However, we cannot rule out that the 2D averages could actually be showing the same face in alternative conformations; higher-resolution data will therefore be necessary to resolve these models.

DISCUSSION

In this study, we used biochemical, genetic and structural methods to dissect the architecture of the yeast exocyst complex and examined mechanisms for its assembly and function. We purified endogenous, intact exocyst complexes from *S. cerevisiae* (**Fig. 1**), and our biochemical and structural characterization demonstrated an intrinsically stable, intact octameric complex (**Figs. 2** and **6**). Our results with the AID system indicated that the presence of most of the exocyst subunits is critical to complex integrity and stability (**Fig. 4**). Degradation of six out of the seven AID-tagged subunits tested, except Sec3, triggered complete separation of the exocyst into two modules (**Fig. 4**). Each of these modules (3–5–6–8 and 10–15–70–84) is assembled by several critical pairwise interactions (3–5, 6–8 and 10–15) with weaker contributions from 5–6, 70–84, 84–10 and 8–10 or 8–15 (**Figs. 2** and **4**); furthermore, the disassembly of one module does not affect the integrity of the other. Consistently with this, our negative-stain EM 2D class averages demonstrated a stable, homogenous, octameric complex (**Fig. 6**). The assembly and stability of the exocyst structure is independent of the known binding partners Sec4, Snc1/2, Myo2, Sec1 and Cdc42 (**Fig. 5**). These components are not stable, stoichiometric partners of the exocyst complex, nor is their binding necessary to assemble or stabilize the exocyst complex during vesicle transport, tethering or fusion. We propose that the role of these interactions is to modulate the function, rather than the assembly, of the exocyst complex.

Our results do not support previous hypotheses that have suggested a requirement for polarized vesicle transport in driving the assembly of a subcomplex of exocyst subunits (for example, Sec15–Sec10–Sec6–Sec8–Exo84) on vesicles with a subgroup (Sec3 and Exo70) serving as a 'landmark' on the plasma membrane; assembly of these two subgroups would subsequently drive vesicle tethering[28]. Under physiological conditions, we did not detect any stable subcomplexes in our pulldowns. It is possible that we detected only stoichiometric complexes because uncomplexed subunits or unstable subcomplexes are degraded during the purification; however, our biochemical and AID experiments do not support this possibility, because we could easily purify individual subunits and subcomplexes from yeast lysate with a yield equal to that of assembled complexes (**Figs. 2** and **4**). Furthermore, under conditions in which we disrupted vesicle transport, cell polarity and exocyst binding to vesicles, no subcomplexes were detectable (**Fig. 5**). We cannot rule out the presence of either low levels of subcomplexes or free pools of exocyst subunits below our limit of detection (<5–10%), however, the majority of the exocyst exists in the fully assembled state. In contrast, subcomplexes appear to be present in mammalian cells: the components identified thus

© 2015 Nature America, Inc. All rights reserved.

far (Exo84–Sec10 and Sec5–Sec6 in opposing groups) are consistent with the modules identified here[55,56]. Similarly, differences in subunit localization patterns in the growing hyphae of *Neurospora crassa*, in *A. thaliana* and in different *Drosophila melanogaster* tissues suggest putative subgroups of exocyst subunits[14,57,58]. Regulated assembly and disassembly of the exocyst in different organisms may be an important mechanism by which the exocyst complex participates in a diverse array of processes in a variety of cell types.

Negative-stain EM revealed the first evidence, to our knowledge, of the ellipsoid-shaped structure of the yeast exocyst complex, with its distinct helical bundle–shaped legs packed together (**Fig. 6**). Overall, the yeast exocyst structure is roughly similar to those of the mammalian exocyst complexes previously imaged with rotary shadowing EM[32]. However, unlike the individual Y-shaped structures observed with glutaraldehyde-fixed mammalian exocyst particles, our yeast 2D averages do not appear to have the same short 'arms'. The arms may be too flexible or heterogeneous to be observed in our 2D averages or may represent mammalian-specific domains (for example, Ral-binding domains in Sec5 and Exo84); alternatively, perhaps the mammalian exocyst was partially disassembled during processing. Future efforts will require the use of higher-resolution data and other strategies to uniquely identify each exocyst subunit within the structure.

Members of the CATCHR family of MTCs, including the exocyst, COG, GARP and Dsl1, share functional similarity as well as structural similarity at the individual subunit level. Thus, they might be expected to assemble into comparable quaternary structures, although they contain different numbers of subunits[3]. Similarly to the exocyst modules identified here, COG consists of two structurally and functionally distinct subassemblies with four subunits each[59]. However, in terms of their overall shapes, as determined by negative-stain EM, the exocyst differs markedly from that of both COG and Dsl1. The COG and Dsl1 structures consist of ~3-nm-wide legs emanating from a central flexible 'joint'[59,60], whereas the exocyst's legs fold alongside each other to form a compact ellipsoid structure. It is possible that the COG and Dsl1 complexes might adopt more compact structures with all their subunits present or that they might represent a different, biologically relevant conformation that is not captured in the exocyst EM particles. It will be interesting to determine whether there is a conserved distance for vesicle capture by MTCs at the target membrane and whether all MTCs undergo conformational changes to bring vesicles into closer proximity for SNARE assembly and vesicle fusion, as has previously been suggested for the Dsl1 complex[60].

We propose that, in contrast with models proposing that assembly of subcomplexes is required for exocyst function, the yeast exocyst complex functions as a stably assembled octamer in the cell. The subunits pack together into an elongated structure. This structure could be a single conformation that functions through changing interactions with various partner proteins. Alternatively, the exocyst may undergo conformational changes in response to binding its protein or membrane partners. Defining the subunit positions and binding of partners at higher resolution is necessary for elucidating the mechanisms of vesicle tethering and SNARE-complex regulation at the plasma membrane. This knowledge is also critical in determining whether the MTCs function by similar mechanisms and how they are uniquely suited to specific trafficking pathways and cell types. Importantly, the ability to purify stable yeast exocyst complexes will now enable functional studies to obtain a detailed molecular understanding of the exocyst's role in vesicle tethering and SNARE-complex regulation.

METHODS

Methods and any associated references are available in the online version of the paper.

Note: Any Supplementary Information and Source Data files are available in the online version of the paper.

ACKNOWLEDGMENTS

We thank P. Brennwald (University of North Carolina, Chapel Hill), C. Carr (Texas A&M University) and L. Weisman (University of Michigan) for antibodies, P. Novick (University of California, San Diego) for gifts of yeast strains, the Yeast Genome Resource Center in Japan for the AID-system reagents and the Wendland laboratory (Johns Hopkins University) for technical advice. Thanks to W. Holmes, M. Jacques, R. Kalia, L. Hassinger and members of the University of Massachusetts Medical School Core EM Facility for technical assistance. Thanks to R. Gilmore, S. Ryder, P. Pryciak, C. Carr and members of M.M.'s laboratory for critical reading of this manuscript and advice. Work in our laboratories is supported by US National Institutes of Health grants GM068803 (M.M. and A.F.), 1DP2GM110772 (A.F.), U54 GM103511 and P41 GM109824 (M.P.R.), and a Searle Scholars Award (A.F.).

AUTHOR CONTRIBUTIONS

M.R.H. and M.M. conceived the study, designed the biochemical and cell biology experiments and wrote the manuscript; M.R.H. made yeast strains and performed most of the biochemistry and cell biology experiments with assistance from A.M.M., C.M.D., L.L.M. and A.C.W.; M.G. and A.F. designed, performed and analyzed the EM experiments; early EM optimization work was done by N.F.; development of the purification method was done by Z.H., C.M.D., M.P.R. and M.C.F.; all authors contributed to discussion and approved the final manuscript.

COMPETING FINANCIAL INTERESTS

The authors declare no competing financial interests.

Reprints and permissions information is available online at http://www.nature.com/reprints/index.html.

1. Heider, M.R. & Munson, M. Exorcising the exocyst complex. *Traffic* **13**, 898–907 (2012).
2. Wickner, W. & Schekman, R. Membrane fusion. *Nat. Struct. Mol. Biol.* **15**, 658–664 (2008).
3. Yu, I.M. & Hughson, F.M. Tethering factors as organizers of intracellular vesicular traffic. *Annu. Rev. Cell Dev. Biol.* **26**, 137–156 (2010).
4. Chia, P.Z. & Gleeson, P.A. Membrane tethering. *F1000Prime Rep.* **6**, 74 (2014).
5. Brunet, S. & Sacher, M. Are MTCs tethering complexes or trafficking complexes that may act as tethers? *Traffic* **15**, 1282–1287 (2014).
6. Sivaram, M.V., Saporita, J.A., Furgason, M.L.M., Boettcher, A.J. & Munson, M. Dimerization of the exocyst protein Sec6p and its interaction with the t-SNARE Sec9p. *Biochemistry* **44**, 6302–6311 (2005).
7. Morgera, F. *et al.* Regulation of exocytosis by the exocyst subunit Sec6 and the SM protein Sec1. *Mol. Biol. Cell* **23**, 337–346 (2012).
8. Laufman, O., Hong, W. & Lev, S. The COG complex interacts with multiple Golgi SNAREs and enhances fusogenic assembly of SNARE complexes. *J. Cell Sci.* **126**, 1506–1516 (2013).
9. TerBush, D.R., Maurice, T., Roth, D. & Novick, P. The Exocyst is a multiprotein complex required for exocytosis in *Saccharomyces cerevisiae*. *EMBO J.* **15**, 6483–6494 (1996).
10. TerBush, D.R. & Novick, P. Sec6, Sec8, and Sec15 are components of a multisubunit complex which localizes to small bud tips in *Saccharomyces cerevisiae*. *J. Cell Biol.* **130**, 299–312 (1995).
11. Guo, W., Grant, A. & Novick, P. Exo84p is an exocyst protein essential for secretion. *J. Biol. Chem.* **274**, 23558–23564 (1999).
12. Hsu, S.C. *et al.* The mammalian brain rsec6/8 complex. *Neuron* **17**, 1209–1219 (1996).
13. Koumandou, V.L., Dacks, J.B., Coulson, R.M. & Field, M.C. Control systems for membrane fusion in the ancestral eukaryote; evolution of tethering complexes and SM proteins. *BMC Evol. Biol.* **7**, 29 (2007).
14. Riquelme, M. *et al.* The *Neurospora crassa* exocyst complex tethers Spitzenkörper vesicles to the apical plasma membrane during polarized growth. *Mol. Biol. Cell* **25**, 1312–1326 (2014).
15. Novick, P., Field, C. & Schekman, R. Identification of 23 complementation groups required for post-translational events in the yeast secretory pathway. *Cell* **21**, 205–215 (1980).
16. Guo, W., Roth, D., Walch-Solimena, C. & Novick, P. The exocyst is an effector for Sec4p, targeting secretory vesicles to sites of exocytosis. *EMBO J.* **18**, 1071–1080 (1999).
17. Friedrich, G.A., Hildebrand, J.D. & Soriano, P. The secretory protein Sec8 is required for paraxial mesoderm formation in the mouse. *Dev. Biol.* **192**, 364–374 (1997).

© 2015 Nature America, Inc. All rights reserved.

18. Murthy, M., Garza, D., Scheller, R.H. & Schwarz, T.L. Mutations in the exocyst component Sec5 disrupt neuronal membrane traffic, but neurotransmitter release persists. *Neuron* **37**, 433–447 (2003).
19. Jin, Y. *et al.* Myosin V transports secretory vesicles via a Rab GTPase cascade and interaction with the exocyst complex. *Dev. Cell* **21**, 1156–1170 (2011).
20. Munson, M. & Novick, P. The exocyst defrocked, a framework of rods revealed. *Nat. Struct. Mol. Biol.* **13**, 577–581 (2006).
21. Shen, D. *et al.* The synaptobrevin homologue Snc2p recruits the exocyst to secretory vesicles by binding to Sec6p. *J. Cell Biol.* **202**, 509–526 (2013).
22. Wu, H., Rossi, G. & Brennwald, P. The ghost in the machine: small GTPases as spatial regulators of exocytosis. *Trends Cell Biol.* **18**, 397–404 (2008).
23. Wu, H., Turner, C., Gardner, J., Temple, B. & Brennwald, P. The Exo70 subunit of the exocyst is an effector for both Cdc42 and Rho3 function in polarized exocytosis. *Mol. Biol. Cell* **21**, 430–442 (2010).
24. He, B., Xi, F., Zhang, X., Zhang, J. & Guo, W. Exo70 interacts with phospholipids and mediates the targeting of the exocyst to the plasma membrane. *EMBO J.* **26**, 4053–4065 (2007).
25. Zhang, X. *et al.* Membrane association and functional regulation of Sec3 by phospholipids and Cdc42. *J. Cell Biol.* **180**, 145–158 (2008).
26. Baek, K. *et al.* Structure-function study of the N-terminal domain of exocyst subunit Sec3. *J. Biol. Chem.* **285**, 10424–10433 (2010).
27. Songer, J.A. & Munson, M. Sec6p anchors the assembled exocyst complex at sites of secretion. *Mol. Biol. Cell* **20**, 973–982 (2009).
28. Boyd, C., Hughes, T., Pypaert, M. & Novick, P. Vesicles carry most exocyst subunits to exocytic sites marked by the remaining two subunits, Sec3p and Exo70p. *J. Cell Biol.* **167**, 889–901 (2004).
29. Katoh, Y., Nozaki, S., Hartanto, D., Miyano, R. & Nakayama, K. Architectures of multisubunit complexes revealed by a visible immunoprecipitation assay using fluorescent fusion proteins. *J. Cell Sci.* **128**, 2351–2362 (2015).
30. Terbush, D.R., Guo, W., Dunkelbarger, S. & Novick, P. Purification and characterization of yeast exocyst complex. *Methods Enzymol.* **329**, 100–110 (2001).
31. De Craene, J.O. *et al.* Rtn1p is involved in structuring the cortical endoplasmic reticulum. *Mol. Biol. Cell* **17**, 3009–3020 (2006).
32. Hsu, S.C. *et al.* Subunit composition, protein interactions, and structures of the mammalian brain sec6/8 complex and septin filaments. *Neuron* **20**, 1111–1122 (1998).
33. Oeffinger, M. *et al.* Rrp17p is a eukaryotic exonuclease required for 5′ end processing of Pre-60S ribosomal RNA. *Mol. Cell* **36**, 768–781 (2009).
34. Hakhverdyan, Z. *et al.* Rapid, optimized interactomic screening. *Nat. Methods* **12**, 553–560 (2015).
35. Richman, D.D., Cleveland, P.H., Oxman, M.N. & Johnson, K.M. The binding of staphylococcal protein A by the sera of different animal species. *J. Immunol.* **128**, 2300–2305 (1982).
36. Oeffinger, M. *et al.* Comprehensive analysis of diverse ribonucleoprotein complexes. *Nat. Methods* **4**, 951–956 (2007).
37. Bowser, R., Müller, H., Govindan, B. & Novick, P. Sec8p and Sec15p are components of a plasma membrane-associated 19.5S particle that may function downstream of Sec4p to control exocytosis. *J. Cell Biol.* **118**, 1041–1056 (1992).
38. Roth, D., Guo, W. & Novick, P. Dominant negative alleles of SEC10 reveal distinct domains involved in secretion and morphogenesis in yeast. *Mol. Biol. Cell* **9**, 1725–1739 (1998).
39. Wiederkehr, A., De Craene, J.O., Ferro-Novick, S. & Novick, P. Functional specialization within a vesicle tethering complex: bypass of a subset of exocyst deletion mutants by Sec1p or Sec4p. *J. Cell Biol.* **167**, 875–887 (2004).
40. Haarer, B.K. *et al.* SEC3 mutations are synthetically lethal with profilin mutations and cause defects in diploid-specific bud-site selection. *Genetics* **144**, 495–510 (1996).
41. Nishimura, K., Fukagawa, T., Takisawa, H., Kakimoto, T. & Kanemaki, M. An auxin-based degron system for the rapid depletion of proteins in nonplant cells. *Nat. Methods* **6**, 917–922 (2009).
42. Nishimura, K. & Kanemaki, M.T. Rapid depletion of budding yeast proteins via the fusion of an auxin-inducible degron (AID). *Curr. Protoc. Cell Biol.* **64**, 20.9 (2014).
43. Adamo, J.E. *et al.* Yeast Cdc42 functions at a late step in exocytosis, specifically during polarized growth of the emerging bud. *J. Cell Biol.* **155**, 581–592 (2001).
44. Hashizume, K., Cheng, Y.S., Hutton, J.L., Chiu, C.H. & Carr, C.M. Yeast Sec1p functions before and after vesicle docking. *Mol. Biol. Cell* **20**, 4673–4685 (2009).
45. Zhang, X. *et al.* Cdc42 interacts with the exocyst and regulates polarized secretion. *J. Biol. Chem.* **276**, 46745–46750 (2001).
46. Donovan, K.W. & Bretscher, A. Myosin-V is activated by binding secretory cargo and released in coordination with Rab/exocyst function. *Dev. Cell* **23**, 769–781 (2012).
47. Novick, P. & Schekman, R. Secretion and cell-surface growth are blocked in a temperature-sensitive mutant of *Saccharomyces cerevisiae*. *Proc. Natl. Acad. Sci. USA* **76**, 1858–1862 (1979).
48. Govindan, B., Bowser, R. & Novick, P. The role of Myo2, a yeast class V myosin, in vesicular transport. *J. Cell Biol.* **128**, 1055–1068 (1995).
49. Croteau, N.J., Furgason, M.L., Devos, D. & Munson, M. Conservation of helical bundle structure between the exocyst subunits. *PLoS One* **4**, e4443 (2009).
50. Wu, S., Mehta, S.Q., Pichaud, F., Bellen, H.J. & Quiocho, F.A. Sec15 interacts with Rab11 via a novel domain and affects Rab11 localization *in vivo*. *Nat. Struct. Mol. Biol.* **12**, 879–885 (2005).
51. Dong, G., Hutagalung, A.H., Fu, C., Novick, P. & Reinisch, K.M. The structures of exocyst subunit Exo70p and the Exo84p C-terminal domains reveal a common motif. *Nat. Struct. Mol. Biol.* **12**, 1094–1100 (2005).
52. Yamashita, M. *et al.* Structural basis for the Rho- and phosphoinositide-dependent localization of the exocyst subunit Sec3. *Nat. Struct. Mol. Biol.* **17**, 180–186 (2010).
53. Hamburger, Z.A., Hamburger, A.E., West, A.P. Jr. & Weis, W.I. Crystal structure of the *S.cerevisiae* exocyst component Exo70p. *J. Mol. Biol.* **356**, 9–21 (2006).
54. Sivaram, M.V., Furgason, M.L.M., Brewer, D.N. & Munson, M. The structure of the exocyst subunit Sec6p defines a conserved architecture with diverse roles. *Nat. Struct. Mol. Biol.* **13**, 555–556 (2006).
55. Moskalenko, S. *et al.* Ral GTPases regulate exocyst assembly through dual subunit interactions. *J. Biol. Chem.* **278**, 51743–51748 (2003).
56. Bodemann, B.O. *et al.* RalB and the exocyst mediate the cellular starvation response by direct activation of autophagosome assembly. *Cell* **144**, 253–267 (2011).
57. Fendrych, M. *et al.* Visualization of the exocyst complex dynamics at the plasma membrane of *Arabidopsis thaliana*. *Mol. Biol. Cell* **24**, 510–520 (2013).
58. Murthy, M. *et al.* Sec6 mutations and the *Drosophila* exocyst complex. *J. Cell Sci.* **118**, 1139–1150 (2005).
59. Lees, J.A., Yip, C.K., Walz, T. & Hughson, F.M. Molecular organization of the COG vesicle tethering complex. *Nat. Struct. Mol. Biol.* **17**, 1292–1297 (2010).
60. Ren, Y. *et al.* A structure-based mechanism for vesicle capture by the multisubunit tethering complex Dsl1. *Cell* **139**, 1119–1129 (2009).

© 2015 Nature America, Inc. All rights reserved.

ONLINE METHODS

Yeast methods. The strains used in this study are listed in **Supplementary Table 1**. Standard methods were used for yeast media and genetic manipulations. Cells were grown in YPD medium containing 1% Bacto-yeast extract (Fisher Scientific), 2% Bacto-peptone (Fisher Scientific), and 2% glucose (Sigma-Aldrich). All protein A (PrA) tags were integrated at the genomic loci in haploid yeast strains (BY4741 or BY4742) by integration of linear PCR products. PrA products were amplified from a plasmid (pProtAHIS5, M.P.R.'s laboratory) encoding a PreScission Protease (PPX) site upstream of the PrA tag and a *Schizosaccharomyces pombe HIS5* selection marker[36]. Approximately 60 bp of sequence homologous to the 5′ end of the coding sequence and 60 bp of sequence homologous to the 3′ flanking sequence were used for homologous recombination. All exocyst PrA tags were added at the C-terminal ends. AID tags (IAA17) and linker were amplified from BYP6740 (pMK43, Yeast Genome Resource Center (YGRC), Japan). For C-terminal AID-tag strains, tags were added at the genomic locus of the strain BY25598 (YGRC), which expresses OsTIR1 under the ADH1 promoter (parent w303-1a), with linear PCR products and *kanMX* selection. N-terminal AID tags (*SNC2*, *SEC4*, and *CDC42* only) were integrated at the genomic locus of BY4742 with the pRS306 integrating plasmid[61]. Inserts were amplified by overlap extension of PCR products to generate a product consisting of ~300 bp of 5′ regulatory element, AID tag, linker, and sequence matching the 5′ end of the gene of interest, and this was then inserted into pRS306 through NotI and XhoI restriction sites. The plasmids were linearized with restriction enzymes specific to the 5′ regulatory elements of each gene (*SNC2*, MluI; *SEC4*, BsrGI; *CDC42*, HpaI) before yeast transformation. For the AID-Snc2 strain, *SNC1* was deleted by replacing the genomic locus with the *kanMX* cassette. Finally, for all N-terminal AID-tag strains, the OsTIR1 gene was integrated at the *MET15* locus with a *URA3* marker and an *ADH1* promoter. The plasmid BYP6744 (pNHK53, YGRC) was used as a template for generating the OsTIR1 PCR product, and sequence homologous to the *MET15* regulatory elements was added to the ends. For serial-dilution growth assays, yeast cells were grown in YPD to an OD of 1.5 and serially diluted ten-fold across YPD plates or YPD plates containing the indicated concentrations of IAA (VWR). Yeast plates were incubated at 30 °C for 2 d before imaging on Fujifilm LAS3000 (GE).

Exocyst protein A purification. Yeast cells (2 L) were grown in YPD at 30 °C to an OD of 1.3–1.5. Cells were washed with water, extruded through a syringe as frozen noodles into liquid nitrogen, and stored at −80 °C until lysis[36]. Noodles were lysed in a 50-ml stainless steel Komfort jar with stainless-steel ball bearings, prechilled in liquid nitrogen with a PM100 machine (Retsch). The resulting yeast powder was stored at −80 °C. 150 mg of yeast powder was added to 1.5-ml microcentrifuge tubes prechilled in liquid nitrogen. 600 µl of resuspension buffer (50 mM HEPES, pH 7.4, and 150 mM NaCl unless noted otherwise in the text, with 1× complete Mini EDTA-free protease-inhibitor solution (Roche Life Science)) was added to the tube (with buffer composition varying by experiment, as noted in the relevant figures) and was then vortexed and pipetted briefly to achieve complete resuspension. Spheroplasting and bead-beating lysis were performed as previously described[7] with 50 mM HEPES, pH 7.4, and 300 mM KCl lysis buffer. The use of NaCl versus KCl had no effect on exocyst preparations. Tubes were spun at 14,000*g* for 10 min at 4 °C, and the supernatant was added to 5 µl homemade rabbit IgG magnetic bead slurry[34,36]. Binding was carried out for 45 min at 4 °C on a nutating platform. The beads were washed in resuspension buffer and eluted either in 1× SDS loading buffer or by 1 h treatment with PreScission Protease (GE Healthcare) at 4 °C for a native elution. Samples were run on SDS-PAGE and stained with Coomassie Blue or Krypton fluorescent protein stain (Thermo Fisher Scientific). Western blot analyses were performed with rabbit polyclonal antibodies to Sec6, Sec8, Sec10, Exo70, and Exo84 (refs. 7,27). Rabbit polyclonal antibodies to Sec3, Sec15, and Sec5, and mouse monoclonal antibodies to Cdc42 and Sec4 were gifts from P. Brennwald (University of North Carolina, Chapel Hill). Rabbit polyclonal antibodies to Sec1 and Snc were gifts from C. Carr (Texas A&M University). Goat polyclonal antibody to Myo2 was a gift from L. Weisman (University of Michigan). Rabbit polyclonal antibody to ADH was purchased from Abcam (ab20994). Mouse monoclonal antibody to GFP was purchased from Clontech (632380). Western blot analyses of exocyst protein levels in input versus unbound samples showed that ~60% of exocyst complexes were bound to the beads (varying slightly by bead preparation). The IgG beads were saturated in these experiments, however, because the exocyst complexes remaining in the lysates could be pulled down by sequential bead incubations. Krypton staining of the resulting gels showed no differences in stoichiometry in sequential pulldowns of either Sec5-PrA or Sec15-PrA. Coomassie-stained gels were imaged on an LAS 4000 (GE Healthcare Life Sciences), and Krypton gels were imaged on a Typhoon FLA9000 (GE Healthcare Life Sciences). Western blots were treated with ECL and imaged on an LAS 4000. Full-size gels and western blots are available in **Supplementary Data Set 1**.

Auxin-induced degradation of exocyst subunits and exocyst regulators. Yeast cells (2 L) were grown in YPD at 30 °C to an OD of 1.0. IAA (VWR), dissolved in 100% ethanol at 500 mM, was added to yeast cultures for a final concentration of 0.7 mM. The cells were allowed to grow in IAA for 45 min (with 15 min for post-processing) at 30 °C until an OD of about 1.5 was reached. The cells were then washed with water, harvested as frozen noodles, and lysed as described above in the purification section. NaOH/SDS lysis was used for visualizing IAA-induced degradation in yeast lysates for **Figure 3c** and **Supplementary Figure 3**. Briefly, 2.5 OD units of yeast was incubated in 100 mM NaOH for 5 min, centrifuged to remove the NaOH, resuspended in SDS loading buffer with DTT, and heated at 95 °C before loading onto gels for SDS-PAGE and western blotting.

Bgl2 secretion assay. AID strains were grown at 30 °C in YPD and treated for 1 h with 0.7 mM IAA before harvesting. Bgl2 secretion assays were performed as described in Adamo *et al.*[62]. Internal Bgl2 levels were quantified by western blotting and normalized to internal ADH levels. All strains were normalized relative to internal Bgl2 levels of the appropriate untreated wild-type-strain control.

Thin-section electron microscopy. EM on wild-type and AID-tagged yeast strains was performed as previously described[63]. Briefly, yeast cells were grown in YPD at 30 °C and treated with 0.7 mM IAA for 1 h. 10 OD units were harvested, fixed for 1 h at room temperature with 3% glutaraldehyde, 2.5% sucrose, 5 mM $CaCl_2$, and 5 mM MgCl in 0.1 M sodium cacodylate, pH 7.4. Cells were spheroplasted with buffer containing 10% β-glucuronidase and 0.5 mg/ml zymolyase for 30 min at 30 °C, washed in 0.1 M cacodylate/1 M sorbitol, resuspended in 0.1 M sodium cacodylate, pH 6.8/1 M sorbitol, and embedded in 2% agarose. Agarose pieces were stained with 1% OsO_4 and 1% potassium ferrocyanide in 0.1 M sodium cacodylate, pH 6.8, for 30 min, then washed completely and stained in 1% thiocarbohydrazide for 5 min at room temperature. After being washed completely, samples were treated for 5 min with 1% OsO_4/1% potassium ferrocyanide and washed again. After ethanol dehydration and embedding in Epon resin (Electron Microscopy Science), thin sections were cut at 70 nm and added to uncoated copper grids. Grids were post-stained with uranyl acetate and lead citrate. Samples were viewed on a Philips CM10 at 80 kV and recorded with a Gatan Erlangshen 785 CCD digital camera.

Negative-stain electron microscopy and image analysis. Sec15-PrA and Sec15-GFP–Sec6-PrA complexes were purified in 20 mM PIPES, pH 6.8, and 300 mM KCl. The complexes were released from IgG beads after PPX cleavage to produce purified wild-type and Sec15-GFP complexes. Those complexes were absorbed to glow-discharged carbon-coated copper grids and stained with 1% uranyl acetate. Micrographs of wild-type complex were collected on an FEI Tecnai F20 electron microscope operated at 200 kV and 20,400× nominal magnification. The defocus value ranged from 0.5 to 2.0 µm. Images were collected with a Gatan K2 summit direct detector with final pixel size of 2.45 Å. We semiautomatically picked 67,509 Sec15-GFP particles and 24,891 wild-type particles, and performed grayscale normalization with Relion-1.3 (ref. 64). Micrographs of the Sec15-GFP complex were collected on an FEI Titan Krios electron microscope operated at 300 kV and 29,000× nominal magnification. The defocus value ranged from 0.5 to 3.0 µm. Images were collected automatically with EPU (FEI) with final pixel size of 2.87 Å. Particles were selected manually and grayscale normalized with BOXER as implemented in EMAN2 (ref. 65). For the Sec15-GFP data set, there were 2,568 unique micrographs and 67,509 particles picked; 60,751 particles survived. For the untagged wild-type data set, there were 298 unique micrographs and 24,891 particles picked; 17,420 particles survived. Contrast transfer function (CTF) estimation was performed with CTFFIND3 (ref. 66). CTF correction, 2D classification and averaging were performed via Maximum a posteriori refinement as implemented in RELION[64]. The negative-stain EM data are available upon request.

© 2015 Nature America, Inc. All rights reserved.

61. Sikorski, R.S. & Hieter, P. A system of shuttle vectors and yeast host strains designed for efficient manipulation of DNA in *Saccharomyces cerevisiae*. *Genetics* **122**, 19–27 (1989).
62. Adamo, J.E., Rossi, G. & Brennwald, P. The Rho GTPase Rho3 has a direct role in exocytosis that is distinct from its role in actin polarity. *Mol. Biol. Cell* **10**, 4121–4133 (1999).
63. Perkins, E.M. & McCaffery, J.M. in *Mitochondria* 467–483 (Springer, 2007).
64. Scheres, S.H. RELION: implementation of a Bayesian approach to cryo-EM structure determination. *J. Struct. Biol.* **180**, 519–530 (2012).
65. Ludtke, S.J., Baldwin, P.R. & Chiu, W. EMAN: semiautomated software for high-resolution single-particle reconstructions. *J. Struct. Biol.* **128**, 82–97 (1999).
66. Mindell, J.A. & Grigorieff, N. Accurate determination of local defocus and specimen tilt in electron microscopy. *J. Struct. Biol.* **142**, 334–347 (2003).

© 2015 Nature America, Inc. All rights reserved.

doi:10.1038/nsmb.3146